

# A Generalized Space-Time CE/SE Method for the Euler Equations on Quadrilateral and Hexagonal Meshes

Zeng-Chan Zhang<sup>1</sup> and S.T. John Yu<sup>2</sup>

Mechanical Engineering Department

Wayne State University

Detroit, MI 48202

## Abstract

In this paper, we report a variation of the Space-Time Conservation Element and Solution Element (CE/SE) method, originally developed by Chang [1-5] for solving conservation laws. In the present method, a single conservation element at each grid point is employed for solving conservation laws no matter in one, two, and three spatial dimensions, instead of two in one-dimensional, three in two-dimensional, and four in three-dimensional problems, as proposed by Chang. As a contrast to Chang's approach, the conservation element here is used to calculate flow variables only, whilst the gradients of flow variables are calculated by a central-differencing reconstruction procedure. For equations in one spatial dimension, the present approach is a special case of Chang's  $a$ - $\epsilon$  scheme. For equations in two and three spatial dimensions, the present method can be easily applied to a regular structured mesh. As such, the present method can be adopted as an alternative solver for time-accurate solutions in well-established CFD codes. Nevertheless, the present scheme inherits most of the advantageous features of the original CE/SE method, including efficient operational count, easiness of implementing non-reflective boundary condition, and high-fidelity resolution of wave motions. In particular, the Godunov type methods using Riemann solvers, i.e., the paradigm of modern upwind schemes, are not needed to capture shocks. Therefore, the computational logic is considerably simpler. To demonstrate the capability of the present method, numerical results of some benchmark problems are presented, including oblique shock reflection, supersonic flow over a wedge, and a three-dimensional detonating flow.

## 1. Introduction

The Space-Time Conservation Element and Solution Element Method, or the CE/SE Method, originally proposed by Chang [1-5], is a new numerical framework for conservation laws. This method is not an incremental improvement of a previously existing CFD method, and

it differs substantially from other well-established methods. The CE/SE method has many non-traditional features, including a unified treatment of space and time, the introduction of conservation element (CE) and solution element (SE), and a novel shock capturing strategy without using Riemann solvers. To date, numerous highly accurate solutions have been obtained [1-14, 17], including traveling and interacting shocks, acoustic waves, shedding vortices, detonation waves, shock/acoustic waves interaction, shock/vortex interaction, and cavitations. The design principles of the CE/SE method have been extensively illustrated in the cited references.

The CE/SE method is a family of schemes, i.e., the  $a$  scheme, the  $a$ - $\epsilon$  scheme, and the  $a$ - $\alpha$  scheme. The  $a$  scheme determines the space-time geometry of the numerical mesh employed. The  $a$ - $\epsilon$  and the  $a$ - $\alpha$  schemes are extensions of the  $a$  scheme for nonlinear equations and for shock capturing.

In the CE/SE method, the space-time domain of interest is first divided into many Solution Elements (SEs). In each SE, flow variables are assumed continuous. A first-order Taylor series is then used by Chang to discretize the flow variables. Thus the scheme is second-order accurate. Across the boundaries of neighboring SEs, flow discontinuities are allowed. Flow variables are calculated through a local space-time flux balance, which is enforced by integrating over the surfaces of a Conservation Element (CE). Unlike SEs, various CEs could be imposed for local and global space-time flux balance.

In original scheme, the number of the CEs employed marches the number of unknowns designated by the scheme. In addition to the flow variables, the spatial gradients of flow variables are also treated as unknowns. As a result, two CEs are used to solve a one-dimensional conservation equation, because the variable  $u$  and its spatial derivative  $u_x$  are the unknowns. Similarly, three CEs are used for two-dimensional equations, because  $u$ ,  $u_x$ , and  $u_y$  are the unknowns, and

<sup>1</sup> Research Associate, Email: [zhangzc@me1.eng.wayne.edu](mailto:zhangzc@me1.eng.wayne.edu); Phone: (313) 577-3892; Fax: (313) 577-8789

<sup>2</sup> Associate Professor, Email: [sty@eng.wayne.edu](mailto:sty@eng.wayne.edu); Phone: (313) 577-3796; Fax: (313) 577-8789

four CEs are used for the three-dimensional conservation equation. As shown by Chang, triangles and tetrahedrons are used as the basic mesh stencil to construct the necessary CEs for two- and three-dimensional equations. We remark that unlike the modern upwind schemes, flow variable distribution inside a SE is not calculated through a reconstruction procedure using its neighboring values at the same time level. Instead, they are calculated as a part of local space-time flux conservation.

In this paper, the original CE/SE method is modified such that only one CE at each grid point is employed for equations in one, two and three spatial dimensions. As a contract to the original CE/SE method, the CE in the present method is used only to calculate the flow variables, while the spatial gradients of the flow variables are calculated by a central differencing method. For equations in two spatial dimensions, the present method allows the use of quadrilaterals and/or polygons in either structured or unstructured meshes. For equations in three spatial dimensions, general polyhedrons can be used as basic mesh shapes. Thus, the present modified CE/SE method is applicable to general unstructured meshes with mixed elements of various shapes. As such, it can serve as an alternative solver for time-accurate solutions in well-established CFD codes. The rest of the paper is organized as follows.

In Sec. 2, we introduce the modified space-time CE/SE method for the Euler equations in two spatial dimensions. In Sec. 3, the modified CE/SE method is extended to three spatial dimensions. In Sec. 4, numerical examples will be presented to demonstrate the capabilities of the present method. We then offer the concluding remarks and give cited references.

## 2. The Modified CE/SE Method for 2D Euler Equations

Consider the two-dimensional unsteady Euler equations of a perfect gas:

$$\frac{\partial u_m}{\partial t} + \frac{\partial f_m}{\partial x} + \frac{\partial g_m}{\partial y} = 0, \quad (2.1)$$

where  $m=1, 2, 3$ , and  $4$  indicates the four equations ( $u_1=\rho$ ,  $u_2=\rho u$ ,  $u_3=\rho v$ ,  $u_4=E$ ). Following Chang's treatment of space and time, we let  $x_1=x$ ,  $x_2=y$ , and  $x_3=t$  be the coordinates of a three-dimensional Euclidean space  $E_3$ . As such, Eq. (2.1) is equivalent to the integral equation:

$$\oint_{S(V)} \vec{h}_m \cdot d\vec{s} = 0, \quad m=1, 2, 3, 4 \quad (2.2)$$

where  $S(V)$  is the boundary of an arbitrary space-time region  $V$  in  $E_3$ , and the space-time current vector  $\vec{h}_m =$

$(f_m, g_m, u_m)$ . Equation (2.2) is enforced over a space-time region, named conservation element (CE), in which discontinuities of flow variables are allowed. The actual numerical calculation is carried out in a discrete sense by using solution elements (SEs), in which the flow variables are assumed smooth and can be approximated by a specified function.

In the original CE/SE method, the number of CEs associated with each grid point must be identical to the number of the unknowns. In the present approach, however, only one CE associated with each grid point is used for solving the flow variables  $u_m$  in one, two, and three spatial dimensions. The calculations of spatial derivatives  $u_{mx}$  and  $u_{my}$  will be based on a central difference reconstruction procedure.

### 2.1 The Space-Time Geometry of the CE and SE

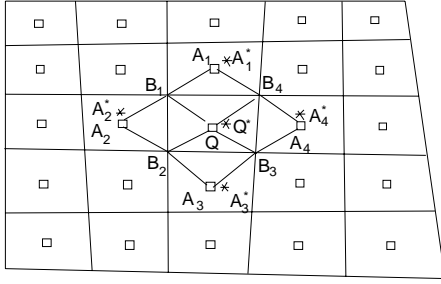
To proceed, we define CEs and SEs in the modified CE/SE method. First, the entire computational domain is divided into non-overlapping quadrilateral cells. Refer to Fig. 2.1 (a). The centroid of each cell is denoted by a square symbol, which is also the grid point in the modified CE/SE method, e.g., point Q in Fig. 2.1. The set of these points is denoted as  $\Omega$ . At each grid point, we construct one CE and one associated SE.

The grid points  $Q, A_1, A_2, A_3$  and  $A_4$  are at time level  $t = t^n$ , where new numerical solutions of flow variables are calculated. Points  $Q', A_1', A_2', A_3'$  and  $A_4'$  are the corresponding points at time level  $t = t^{n-1/2}$ , and points  $Q'', A_1'', A_2'', A_3''$  and  $A_4''$  are at time level  $t = t^{n+1/2}$ . Hereto forth, the above rule is applied to all mesh nodes for denoting the time level, i.e., the superscript ' for  $t = t^{n-1/2}$ , and the superscript '' for  $t = t^{n+1/2}$ . Associated with point Q, the SE(Q) is defined as the union of the quadrilateral cylinder  $B_1'B_2'B_3'B_4'B_1''B_2''B_3''B_4''$  and a horizontal mid plane  $A_1B_1A_2B_2A_3B_3A_4B_4$ . Refer to Fig. 2.1(b).

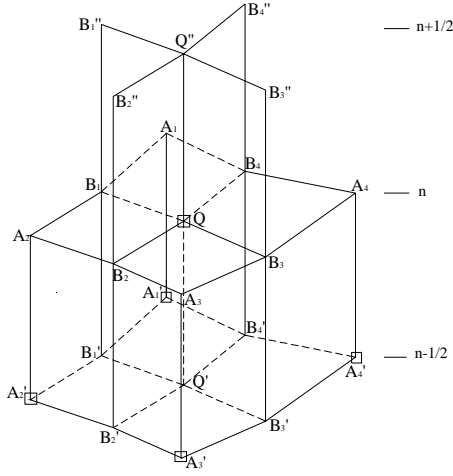
The CE(Q) associated with the point Q is defined as the cylinder  $A_1B_1A_2B_2A_3B_3A_4B_4 A_1'B_1'A_2'B_2'A_3'B_3'A_4'B_4'$ . Refer to Fig. 2.1(b). The centroid of the top surface of this CE, i.e., the polygon  $A_1B_1A_2B_2A_3B_3A_4B_4$ , is used as the solution point, which is denoted by  $Q^*$ . All flow variables and their spatial derivatives are solved and stored at point  $Q^*$ . The set of the solution points is denoted as  $\Omega^*$ . In general, point  $Q^*$  is different from point Q.

The flow variables are assumed smooth inside the SE, and the structure of the flow solution can be discretized by a prescribed function. Following Chang's approach, we discretize the flow variables by the first order Taylor series expansion. That is, for any  $(x, y, t) \in$

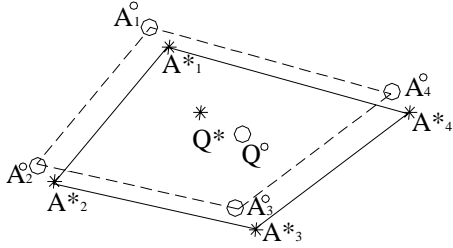
$SE(Q)$ ,  $u_m(x, y, t)$ ,  $f_m(x, y, t)$  and  $g_m(x, y, t)$  are approximated by:



(a)



(b)



(c)

Fig. 2.1: The space-time geometry of the modified CE/SE method: (a) representative grid points in an x-y plane, (b) the definitions of CE and SE, and (c) the parallel translation of the quadrilateral  $A_1^*A_2^*A_3^*A_4^*$ .

$$w_m^*(x, y, t) = (w_m)_{Q^*} + (w_{mx})_{Q^*}(x - x_{Q^*}) + (w_{my})_{Q^*}(y - y_{Q^*}) + (w_{mt})_{Q^*}(t - t^n) \quad (2.3)$$

Where  $w$  can be function  $u, f, g$  or  $q$ , and  $x_{Q^*}, y_{Q^*}$ , and  $t^n$  are the space-time coordinates of  $Q^*$ . Variables  $w_m, w_{mx}, w_{my}$  and  $w_{mt}$  on the left hand side of (2.3) are the discretized variables. If all these values are known, the flow solution structure inside the SE is fully specified. However, the above twelve variables are not totally independent. First, by employing Eq. (2.1), we have

$$(u_{mt})_{Q^*} = -(f_{mx})_{Q^*} - (g_{my})_{Q^*} \quad (2.4a)$$

Second, by applying the chain rule, the spatial and temporal derivatives can be calculated by the corresponding Jacobian matrices multiplied by  $(u_{mx})_{Q^*}$ ,  $(u_{my})_{Q^*}$ , or  $(u_{mt})_{Q^*}$ . For example,

$$(f_{mx})_{Q^*} = (A_{mn})_{Q^*}(u_{nx})_{Q^*} \quad (2.4b)$$

$$(g_{mx})_{Q^*} = (B_{nm})_{Q^*}(u_{nx})_{Q^*} \quad (2.4c)$$

where  $n, m = 1, 2, 3, 4$ , and  $(A_{nm})_{Q^*}$  and  $(B_{nm})_{Q^*}$  are the elements of the Jacobian matrices of  $f_m$  and  $g_m$  calculated at  $Q^*$ . It is similar for  $(f_{my})_{Q^*}$ ,  $(g_{my})_{Q^*}$ ,  $(f_{mt})_{Q^*}$ , and  $(g_{mt})_{Q^*}$ . As a result, the only independent discrete variables in each SE are  $(u_m)_{Q^*}$ ,  $(u_{mx})_{Q^*}$ , and  $(u_{my})_{Q^*}$ . Once these three variables are calculated, the flow solution structure inside the SE is completely determined.

## 2.2 The Calculation of $u_m$

To proceed, the discretized space-time current flux vector

$$\vec{h}_m^*(x, y, t) = (f_m^*(x, y, t), g_m^*(x, y, t), u_m^*(x, y, t)) \quad (2.5)$$

Thus, the space-time flux conservation, Eq. (2.2), can be approximated by its discrete counterpart:

$$\oint_{S(CE(Q))} \vec{h}_m^* \cdot ds = 0 \quad (2.6)$$

Substituting Eqs. (2.3), (2.4), and (2.5) into Eq. (2.6), we obtain the algebraic equation,

$$(u_m)_{Q^*}^n = \left( \sum_{l=1}^4 R_m^{(l)} \right) / S \quad (2.7)$$

Where

$$R_m^{(l)} = S_q^{(l)} \left[ (u_m)_{A_i^*}^{n-1/2} + (x_q^{(l)} - x_{A_i^*})(u_{mx})_{A_i^*}^{n-1/2} + (y_q^{(l)} - y_{A_i^*})(u_{my})_{A_i^*}^{n-1/2} \right] - \sum_{k=1}^2 n_{kx}^{(l)} \left[ (f_m)_{A_i^*}^{n-1/2} + (x_k^{(l)} - x_{A_i^*})(f_{mx})_{A_i^*}^{n-1/2} + (y_k^{(l)} - y_{A_i^*})(f_{my})_{A_i^*}^{n-1/2} + \Delta t / 4 \cdot (f_{mt})_{A_i^*}^{n-1/2} \right] - \sum_{k=1}^2 n_{ky}^{(l)} \left[ (g_m)_{A_i^*}^{n-1/2} + (x_k^{(l)} - x_{A_i^*})(g_{mx})_{A_i^*}^{n-1/2} + \right]$$

$$(y_k^{(l)} - y_{A_l^*})(g_{my})_{A_l^*}^{n-1/2} + \Delta t / 4 \cdot (g_{mt})_{A_l^*}^{n-1/2}] \quad (2.8)$$

for  $l=1, 2, 3$ , and  $4$ , indicating the spatial flux contribution from the four neighboring points, and  $m=1,2,3$  and  $4$ , indicating the four flow equations. Equation (2.7) will be used to calculate the numerical solution of  $u_m$  at point  $Q^*$ . In what follows, we illustrate the geometrical treatments in Eqs. (2.7) and (2.8). Refer to Fig. 2.1.

1. The spatial coordinates of the four neighboring solution points, i.e., points  $A_l^*$ , are denoted by  $(x_{A_l^*}, y_{A_l^*})$  for  $l = 1, 2, 3$ , and  $4$ .
2.  $(x_q^{(l)}, y_q^{(l)})$  for  $l=1, 2, 3$ , and  $4$ , are the spatial coordinates of centroids of four quadrilaterals  $A_1B_1QB_4$ ,  $A_2B_2QB_1$ ,  $A_3B_3QB_2$ , and  $A_4B_4QB_3$ , respectively.
3.  $S_q^{(l)}$  for  $l = 1, 2, 3$ , and  $4$  are surface areas of the four quadrilaterals defined in 2.
4.  $\vec{n}_k^{(l)} = (n_{kx}^{(l)}, n_{ky}^{(l)}, 0)$  for  $l = 1, 2, 3$ , and  $4$ , and  $k = 1, 2$ , represent the eight surface vectors of the following eight lateral planes:  $A_1'B_4'A_1B_4$ ,  $A_1'B_1'A_1B_1$ ,  $A_2'B_1'A_2B_1$ ,  $A_2'B_2'A_2B_2$ ,  $A_3'B_2'A_3B_2$ ,  $A_3'B_3'A_3B_3$ ,  $A_4'B_3'A_4B_3$ , and  $A_4'B_4'A_4B_4$ , respectively. Note that the surface vector is defined as the unit outward normal vector (outward from the interior of the CE) multiplied by its area.
5.  $(x_k^{(l)}, y_k^{(l)}, t^{n-1/4})$  for  $l = 1, 2, 3$ , and  $4$ , and  $k = 1, 2$ , are the space-time coordinates of centroids of the eight lateral planes defined in 4.
6.  $S$  is the area of the polygon  $A_1B_1A_2B_2A_3B_3A_4B_4$ , which is also the top surface of the present CE.

We remark that Eqs. (2.7) and (2.8) represent the space-time flux balance over the CE associated with point  $Q$ . The first term at the right hand side of Eq.(2.8) is the space-time flux through the bottom of the CE, contributed by the four neighboring cells at the time level  $n-1/2$ . The remainder four terms, at the right-hand-side of Eq.(2.8), are the space-time fluxes through the eight lateral plans of the present CE, and they are calculated by a inner product between the space-time vector  $(f_m, g_m, u_m)$  and the surface vector  $\vec{n}_k^{(l)} = (n_{kx}^{(l)}, n_{ky}^{(l)}, 0)$ . The fluxes, calculated by the right hand side of (2.8), are balanced by the space-time flux through the top surface (with the area  $S$ ) of the CE. Since linear distribution of the flow variables is assumed, the flux through the top surface is straightforwardly represented by  $(u_m)^n$  at central point  $Q^*$

multiplied by its area  $S$ . Because all flow conditions at the  $n-1/2$  time level are known, Eqs. (2.7) and (2.8) are the explicit method for calculating of  $(u_m)^n$  at point  $Q^*$ .

### 2.3 Calculations of $u_{mx}$ and $u_{my}$

A central difference type reconstruction approach is employed to calculate  $(u_{mx})_{Q^*}$  and  $(u_{my})_{Q^*}$ . First, we perform a parallel translation of the quadrilateral  $A_1^*A_2^*A_3^*A_4^*$ , so that the centroid of the new quadrilateral  $A_1^{\circ}A_2^{\circ}A_3^{\circ}A_4^{\circ}$  coincides with the solution point  $Q^*$ . Refer to Fig. 2.1(c). The centroid of the quadrilateral  $A_1^*A_2^*A_3^*A_4^*$  is denoted as  $Q^{\circ}$ . Let  $\delta x = x_{Q^{\circ}} - x_{Q^*}$ ,  $\delta y = y_{Q^{\circ}} - y_{Q^*}$ , and then we have:

$$x_{A_l^{\circ}} = x_{A_l^*} + \delta x, \quad y_{A_l^{\circ}} = y_{A_l^*} + \delta y \quad (2.9)$$

where  $l=1, 2, 3$ , and  $4$ , denoting the four corners of the quadrilateral. According to the definition of SEs, we calculate  $u_m$  at points  $A_l^{\circ}$  (for  $l = 1, 2, 3$ , and  $4$ ) by the following Taylor series,

$$(u_m)_{A_l^{\circ}}^n = (u_m)_{A_l^*}^{n-1/2} + (x_{A_l^{\circ}} - x_{A_l^*})(u_{mx})_{A_l^*}^{n-1/2} + (y_{A_l^{\circ}} - y_{A_l^*})(u_{my})_{A_l^*}^{n-1/2} + \frac{\Delta t}{2}(u_{mt})_{A_l^*}^{n-1/2} \quad (2.10)$$

where an expansion in time is also included.

By using the values of  $(u_m)_{A_l^{\circ}}^n$ ,  $(u_m)_{A_2^{\circ}}^n$  and  $(u_m)_{Q^*}^n$ , we can get the first pair of the spatial derivatives of the flow variables, i.e.,  $u_{mx}^{(1)}$ ,  $u_{my}^{(1)}$  at point  $Q^*$ :

$$u_{mx}^{(1)} = \Delta_{mx} / \Delta, \quad u_{my}^{(1)} = \Delta_{my} / \Delta \quad (2.11)$$

where

$$\Delta = \begin{vmatrix} \delta x_1 & \delta y_1 \\ \delta x_2 & \delta y_2 \end{vmatrix}, \quad \Delta_{mx} = \begin{vmatrix} \delta u_m^{(1)} & \delta y_1 \\ \delta u_m^{(2)} & \delta y_2 \end{vmatrix},$$

$$\Delta_{my} = \begin{vmatrix} \delta x_1 & \delta u_m^{(1)} \\ \delta y_1 & \delta u_m^{(2)} \end{vmatrix} \quad (2.12a)$$

$$\delta x_l = (x_{A_l^{\circ}} - x_{Q^*}); \quad \delta y_l = (y_{A_l^{\circ}} - y_{Q^*});$$

$$\delta u_m^{(l)} = [(u_m)_{A_l^{\circ}}^n - (u_m)_{Q^*}^n] \quad (2.12b)$$

Similarly, by using solutions at  $A_2^{\circ}$ ,  $A_3^{\circ}$  and  $Q^*$ , we can get  $u_{mx}^{(2)}$  and  $u_{my}^{(2)}$ . By using solutions at  $A_3^{\circ}$ ,  $A_4^{\circ}$  and  $Q^*$ ,

we get  $u_{mx}^{(3)}$  and  $u_{my}^{(3)}$ . By using solutions at  $A_4^o$ ,  $A_1^o$  and  $Q^*$ , we get  $u_{mx}^{(4)}$  and  $u_{my}^{(4)}$ . Finally, we calculate  $u_{mx}$  and  $u_{my}$  at  $Q^*$  by a simple average:

$$(u_{mx})_{Q^*}^n = (\sum_{k=1}^4 u_{mx}^{(k)})/4, \quad (u_{my})_{Q^*}^n = (\sum_{k=1}^4 u_{my}^{(k)})/4 \quad (2.13)$$

For flows with steep gradients or discontinuities, Eq. (2.13) is modified by a re-weighting procedure:

$$(u_{mx})_{Q^*}^n = \begin{cases} 0, & \text{if } \theta_{ml} = 0, \quad (l=1, 2, 3, 4) \\ \sum_{k=1}^4 [(W_m^{(k)})^\alpha u_{mx}^{(k)}] / \sum_{k=1}^4 (W_m^{(k)})^\alpha, & \text{otherwise} \end{cases}$$

$$(u_{my})_{Q^*}^n = \begin{cases} 0, & \text{if } \theta_{ml} = 0, \quad (l=1, 2, 3, 4) \\ \sum_{k=1}^4 [(W_m^{(k)})^\alpha u_{my}^{(k)}] / \sum_{k=1}^4 (W_m^{(k)})^\alpha, & \text{otherwise} \end{cases} \quad (2.14)$$

Where

$$W_m^{(k)} = \prod_{l=1, l \neq k}^4 \theta_{ml}, \quad \theta_{ml} = \sqrt{(u_{mx}^{(l)})^2 + (u_{my}^{(l)})^2} \quad (2.15)$$

where  $l = 1, 2, 3$ , and  $4$ , and  $m=1, 2, 3$ , and  $4$ . In Eq. (2.14),  $\alpha$  is an adjustable constant. Usually  $\alpha = 1$  or  $2$ . The above re-weighting function is simple and effective to suppress spurious oscillations near shocks. This concludes the formulation of the CE/SE method for the Euler equations in two spatial dimensions. We remark that

1. The present modified CE/SE method is an explicit scheme, which is suitable for parallel computations.

2. For uniform mesh, the grid point  $Q$  coincides with the solution point  $Q^*$ , and the translated point  $Q^o$ . In this case, the above scheme can be greatly simplified.

3. The present scheme is a general framework for both structured and unstructured quadrilateral meshes. For structured meshes, the set of all grid points ( $\Omega$ ) can be divided into two subsets  $\Omega_+$  and  $\Omega_-$ . If a point  $Q$  belongs to  $\Omega_+$  (or  $\Omega_-$ ) its neighbors  $A_1, A_2, A_3$  and  $A_4$  belong to  $\Omega_-$  (or  $\Omega_+$ ). The flow solutions at mesh points in  $\Omega_+$  leapfrog the solutions at mesh points in  $\Omega_-$  in time marching. Therefore, only half of the grid points are needed for each time marching calculation for a half time level, i.e., staggering mesh in time.

4. In general, the above formulation can be easily extended for any polygon shape meshes. Therefore, a calculation method using mixed cells can be developed. For example, one could use triangles to

fill a complex spatial domain, while quadrilaterals could be conveniently used in the near wall regions.

5. For one-dimensional uniform mesh case, the present scheme is a special case of Chang's a-e scheme for  $\varepsilon=0.5$ . According to Chang's analysis, the present scheme is second-order, and the stability constraint is  $CFL \leq 1$ . Interested readers are referred to [1-2] for details of the stability and consistence analyses of the scheme.

### 3. The Modified Space-Time CE/SE Method for 3D Euler Equations

Consider the following three-dimensional Euler equations of a perfect gas:

$$\frac{\partial u_m}{\partial t} + \frac{\partial f_m}{\partial x} + \frac{\partial g_m}{\partial y} + \frac{\partial q_m}{\partial z} = 0 \quad (3.1)$$

where  $m = 1, 2, 3, 4$ , and  $5$ . Let  $x_1 = x, x_2 = y, x_3 = z$ , and  $x_4 = t$  be the coordinates of a four-dimensional Euclidean space  $E_4$ . The corresponding integral equations of Eq. (3.1) are:

$$\oint_{S(V)} \vec{h}_m \cdot d\vec{s} = 0 \quad (3.2)$$

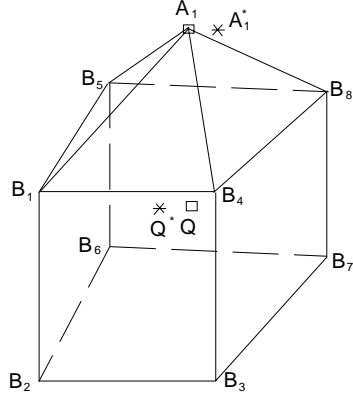
where  $\vec{h}_m = (f_m, g_m, q_m, u_m)$  with  $m=1, 2, 3, 4$ , and  $5$ .  $S(V)$  is the boundary of an space-time region  $V$  in  $E_4$ . In the following, the scheme is illustrated in the following three subsections: (1) definitions of CE and SE, (2) the calculation of  $u_m$ , and (3) calculations of  $u_{mx}, u_{my}$ , and  $u_{mz}$ .

#### 3.1 Definitions of CE and SE

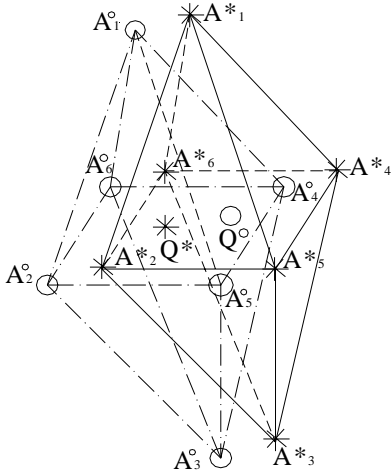
First, the whole computational domain is divided into non-overlapping hexahedrons, in a structured or unstructured mesh. The centroid of each hexahedron is the grid point, which is denoted by a square symbol, e.g., point  $Q$  in Fig. 3.1(a). The set of all these mesh points is denoted as  $\Omega$ . In Fig. 3.1(a), one such hexahedron is plotted, i.e.,  $B_1B_2B_3B_4B_5B_6B_7B_8$ . Obviously, six neighboring hexahedrons and their grid points are connected with this hexahedron. For convenience, only one such neighboring point  $A_1$  is shown in Fig. 3.1(a). The six neighboring grid points connected to  $Q$  are denoted as  $A_1, A_2, A_3, A_4, A_5$  and  $A_6$ . These neighboring hexahedrons share the following common surfaces with the central hexahedron:  $B_1B_4B_8B_5, B_1B_2B_6B_5, B_2B_3B_7B_6, B_3B_7B_8B_4, B_1B_2B_3B_4$  and  $B_5B_6B_7B_8$ .

Note that the grid points  $Q, A_1, A_2, A_3, A_4, A_5$  and  $A_6$  are at time level  $t = t^n$ , where the numerical solutions are calculated. Their corresponding points at

time level  $t = t^{n-1/2}$  are  $Q'$ ,  $A_1'$ ,  $A_2'$ ,  $A_3'$ ,  $A_4'$ ,  $A_5'$  and  $A_6'$ ; and points  $Q''$ ,  $A_1''$ ,  $A_2''$ ,  $A_3''$ ,  $A_4''$ ,  $A_5''$  and  $A_6''$  are at time level  $t = t^{n+1/2}$ .



(a)



(b)

Fig. 3.1: The representative grid points in x-y-z plane and the definitions of CE and SE (a), and the parallel translation (b).

Refer to Fig. 3.1(a). The SE associated with point  $Q$  is defined as the union of the following space-time volumes: (1) a four-dimensional space-time cylinder  $B_1'B_2'B_3'B_4'B_5'B_6'B_7'B_8'B_1''B_2''B_3''B_4''B_5''B_6''B_7''B_8''$ , (2) a spatial volume of the present hexahedron  $B_1B_2B_3B_4B_5B_6B_7B_8$ , and (3) six spatial pyramids:  $A_1B_1B_4B_8B_5$ ,  $A_2B_2B_6B_5B_1$ ,  $A_3B_3B_7B_6B_2$ ,  $A_4B_4B_3B_7B_8$ ,  $A_5B_5B_2B_3B_4$ , and  $A_6B_6B_3B_7B_8$ . Note that the combination of the spatial volumes defined in (2) and (3) is a spatial polyhedron  $A_1B_1B_5A_2B_2B_6A_3B_3B_7A_4B_4B_8A_5A_6$ . Hereto forth, this particular polyhedron is denoted as  $CES(Q)$ .

The CE is defined as a space-time cylinder generated by translating  $CES(Q)$  from  $t = t^{n-1/2}$  to  $t = t^n$ ,

or the space-time volume  $A_1B_1B_5A_2B_2B_6A_3B_3B_7A_4B_4B_8A_5A_6A_1'B_1'B_5'A_2'B_2'B_6'A_3'B_3'B_7'A_4'B_4'B_8'A_5'A_6'$ . Thus  $CES(Q)$  is the projection of the CE into the space at  $t = t^n$ . The centroid of  $CES(Q)$  is defined as the solution point and is denoted by a  $Q^*$ . In general,  $Q^*$  does not coincide with  $Q$ . Flow variables and their spatial derivatives are solved and stored at  $Q^*$ . The set of the solution points is denoted as  $\Omega^*$ .

Inside a SE, the flow solutions are assumed smooth, and we use the first order Taylor series expansion to discretize  $u_m(x, y, z, t)$ ,  $f_m(x, y, z, t)$ ,  $g_m(x, y, z, t)$  and  $q_m(x, y, z, t)$ . That is, for any space-time location inside  $SE(Q)$ , we use the following function to approximate them:

$$\begin{aligned} w_m^*(x, y, z, t) = & (w_m)_{Q^*} + (w_{mx})_{Q^*}(x - x_{Q^*}) \\ & + (w_{my})_{Q^*}(y - y_{Q^*}) + (w_{mz})_{Q^*}(z - z_{Q^*}) \\ & + (w_{mt})_{Q^*}(t - t^n) \end{aligned} \quad (3.3)$$

Here  $w$  can be function  $u$ ,  $f$ ,  $g$  or  $q$ . Thus if all flow solutions, the spatial flux functions, and their spatial and temporal derivatives at  $Q^*$  are known, the entire solution inside the SE is determined. By employing Eq. (3.1), one gets

$$(u_{mt})_{Q^*} = -(f_{mx})_{Q^*} - (g_{my})_{Q^*} - (q_{mz})_{Q^*} \quad (3.4)$$

Similar to that in two spatial dimensions (refer to Sec. 2), the spatial derivatives of flux functions can be calculated by using the flow solutions and their spatial derivatives through using the chain rule. Therefore, in three spatial dimensions, the independent discrete variables at each solution point are  $u_m$ ,  $u_{mx}$ ,  $u_{my}$  and  $u_{mz}$ .

### 3.2 The Calculation of $u_{ma}$

The space-time flux conservation, Eq. (3.2), can be calculated by using its discrete counterpart:

$$\oint_{S(CES(Q))} \vec{h}_m^* \cdot d\vec{S} = 0 \quad (3.5)$$

where the discrete space-time current vector is

$$\begin{aligned} \vec{h}_m^*(x, y, z, t) = & (f_m^*(x, y, z, t), g_m^*(x, y, z, t), \\ & q_m^*(x, y, z, t), u_m^*(x, y, z, t)) \end{aligned} \quad (3.6)$$

Substituting Eqs. (3.3), (3.4), and (3.6) into Eq. (3.5), we obtain

$$(u_m)_{Q^*}^n = \left( \sum_{l=1}^6 R_m^{(l)} \right) / V \quad (3.7)$$

where

$$\begin{aligned}
R_m^{(l)} = & V_q^{(l)} [(u_m)_{A_1^*}^{n-1/2} + (x_q^{(l)} - x_{A_1^*})(u_{mx})_{A_1^*}^{n-1/2} \\
& + (y_q^{(l)} - y_{A_1^*})(u_{my})_{A_1^*}^{n-1/2} + (z_q^{(l)} - z_{A_1^*})(u_{mz})_{A_1^*}^{n-1/2}] \\
& - \sum_{k=1}^4 n_{kx}^{(l)} [(f_m)_{A_1^*}^{n-1/2} + (x_k^{(l)} - x_{A_1^*})(f_{mx})_{A_1^*}^{n-1/2} \\
& + (y_k^{(l)} - y_{A_1^*})(f_{my})_{A_1^*}^{n-1/2} + (z_k^{(l)} - z_{A_1^*})(f_{mz})_{A_1^*}^{n-1/2} \\
& + \Delta t / 4 \cdot (f_m)_{A_1^*}^{n-1/2}] \\
& - \sum_{k=1}^4 n_{ky}^{(l)} [(g_m)_{A_1^*}^{n-1/2} + (x_k^{(l)} - x_{A_1^*})(g_{mx})_{A_1^*}^{n-1/2} \\
& + (y_k^{(l)} - y_{A_1^*})(g_{my})_{A_1^*}^{n-1/2} + (z_k^{(l)} - z_{A_1^*})(g_{mz})_{A_1^*}^{n-1/2} \\
& + \Delta t / 4 \cdot (g_m)_{A_1^*}^{n-1/2}] \\
& - \sum_{k=1}^4 n_{kz}^{(l)} [(q_m)_{A_1^*}^{n-1/2} + (x_k^{(l)} - x_{A_1^*})(q_{mx})_{A_1^*}^{n-1/2} \\
& + (y_k^{(l)} - y_{A_1^*})(q_{my})_{A_1^*}^{n-1/2} + (z_k^{(l)} - z_{A_1^*})(q_{mz})_{A_1^*}^{n-1/2} \\
& + \Delta t / 4 \cdot (q_m)_{A_1^*}^{n-1/2}] \quad (3.8)
\end{aligned}$$

where  $l = 1, 2, 3, 4, 5$ , and  $6$ , denoting the flux contributions from the six neighboring cells, and  $m=1, 2, 3, 4$ , and  $5$  denoting the five unknowns of the three-dimensional Euler equations. The symbols used in Eqs.(3.7) and (3.8) are similar as that in section 2.

The first term on the right hand side of Eq. (3.8) is the calculation of space-time flux through boundary of CE(Q) at  $t = t^{n-1/2}$ . The other terms are the space-time fluxes through the lateral volumes of CE(Q) during the time evolution process. The space-time flux is then balanced by the flux through the boundary of the CE(Q) at  $t = t^n$ , which is simply  $(u_m)_{Q^*}$  multiplied by  $V$ .

### 3.3 Calculations of $u_{mx}$ , $u_{my}$ , and $u_{mz}$

First, the polyhedron  $A_1^* A_2^* A_3^* A_4^* A_5^* A_6^*$  is moved to be  $A_1^o A_2^o A_3^o A_4^o A_5^o A_6^o$ , so that the centroid of the new polyhedron coincides with the solution point  $Q^*$ . Refer to Fig. 3.1(b). Let the centroid of the volume  $A_1^* A_2^* A_3^* A_4^* A_5^* A_6^*$  be denoted as  $Q^o$ , and  $\delta x = x_{Q^*} - x_{Q^o}$ ,  $\delta y = y_{Q^*} - y_{Q^o}$ ,  $\delta z = z_{Q^*} - z_{Q^o}$ , then we have

$$x_{A_1^o} = x_{A_1^*} + \delta x; \quad y_{A_1^o} = y_{A_1^*} + \delta y; \quad z_{A_1^o} = z_{A_1^*} + \delta z \quad (3.9)$$

where  $l=1, 2, 3, 4, 5, 6$ . We can then use the values of  $u_m$  at points  $A_1^o, A_2^o, A_3^o, A_4^o, A_5^o, A_6^o$  and  $Q^*$ , at  $t = t^n$  to calculate the spatial derivatives of flow variables at point  $Q^*$ . For example, by using the values of  $u_m$  at points  $A_1^o, A_2^o, A_5^o$  and  $Q^*$ , i.e.,  $(u_m)_{A_1^o}^n, (u_m)_{A_2^o}^n, (u_m)_{A_5^o}^n$  and  $(u_m)_{Q^*}^n$ , we can calculate  $u_{mx}^{(1)}, u_{my}^{(1)}$ , and  $u_{mz}^{(1)}$ . Note that the superscript  $(1)$  denotes this particular tetrahedron

composed of points  $A_1^o, A_2^o, A_5^o$  and  $Q^*$ . First, we use the Taylor series expansion to get

$$\begin{aligned}
(u_m)_{A_1^o}^n = & (u_m)_{A_1^*}^{n-1/2} + (x_{A_1^o} - x_{A_1^*})(u_{mx})_{A_1^*}^{n-1/2} \\
& + (y_{A_1^o} - y_{A_1^*})(u_{my})_{A_1^*}^{n-1/2} + (z_{A_1^o} - z_{A_1^*})(u_{mz})_{A_1^*}^{n-1/2} \\
& + \Delta t / 2 \cdot (u_m)_{A_1^*}^{n-1/2} \quad (3.10)
\end{aligned}$$

where  $l = 1, 2, 5$ . We can then obtain the following formulation for spatial derivatives  $u_{mx}^{(1)}, u_{my}^{(1)}$  and  $u_{mz}^{(1)}$ :

$$u_{mx}^{(1)} = \Delta_{mx} / \Delta, \quad u_{my}^{(1)} = \Delta_{my} / \Delta, \quad u_{mz}^{(1)} = \Delta_{mz} / \Delta \quad (3.11)$$

where

$$\Delta = \begin{vmatrix} \delta x_1 & \delta y_1 & \delta z_1 \\ \delta x_2 & \delta y_2 & \delta z_2 \\ \delta x_5 & \delta y_5 & \delta z_5 \end{vmatrix}, \quad \Delta_{mx} = \begin{vmatrix} \delta u_m^{(1)} & \delta y_1 & \delta z_1 \\ \delta u_m^{(2)} & \delta y_2 & \delta z_2 \\ \delta u_m^{(5)} & \delta y_5 & \delta z_5 \end{vmatrix} \quad (3.12a)$$

$$\Delta_{my} = \begin{vmatrix} \delta x_1 & \delta u_m^{(1)} & \delta z_1 \\ \delta x_2 & \delta u_m^{(2)} & \delta z_2 \\ \delta x_5 & \delta u_m^{(5)} & \delta z_5 \end{vmatrix}, \quad \Delta_{mz} = \begin{vmatrix} \delta x_1 & \delta y_1 & \delta u_m^{(1)} \\ \delta x_2 & \delta y_2 & \delta u_m^{(2)} \\ \delta x_5 & \delta y_5 & \delta u_m^{(5)} \end{vmatrix} \quad (3.12b)$$

$$\delta x_l = (x_{A_l^o} - x_{Q^*}); \quad \delta y_l = (y_{A_l^o} - y_{Q^*});$$

$$\delta z_l = (z_{A_l^o} - z_{Q^*}) \quad (3.13)$$

$$\delta u_m^{(l)} = [(u_m)_{A_l^o}^n - (u_m)_{Q^*}^n], \quad (3.14)$$

Similarly, by using points other seven sets of points, we can get the other seven similar sets of,  $u_{mx}^{(k)}, u_{my}^{(k)}, u_{mz}^{(k)}$  ( $k=2, 3, 4, 5, 6, 7$ ). Finally, we can obtain the  $u_{mx}, u_{my}$  and  $u_{mz}$  at  $Q^*$  by a simple average procedure:

$$\begin{aligned}
(u_{mx})_{Q^*}^n = & (\sum_{k=1}^8 u_{mx}^{(k)}) / 8, \quad (u_{my})_{Q^*}^n = (\sum_{k=1}^8 u_{my}^{(k)}) / 8 \\
(u_{mz})_{Q^*}^n = & (\sum_{k=1}^8 u_{mz}^{(k)}) / 8 \quad (3.15)
\end{aligned}$$

or the following re-weighting method:

$$(u_{mx})_{Q^*}^n = \begin{cases} 0, & \text{if } \theta_{ml} = 0, \quad (l = 1, 2, 3, 4, 5, 6, 7, 8) \\ \sum_{k=1}^8 [(W_m^{(k)})^\alpha u_{mx}^{(k)}] / \sum_{k=1}^8 (W_m^{(k)})^\alpha, & \text{otherwise} \end{cases} \quad (3.16a)$$

$$(u_{my})_{Q^*}^n = \begin{cases} 0, & \text{if } \theta_{ml} = 0, \quad (l = 1, 2, 3, 4, 5, 6, 7, 8) \\ \sum_{k=1}^8 [(W_m^{(k)})^\alpha u_{my}^{(k)}] / \sum_{k=1}^8 (W_m^{(k)})^\alpha, & \text{otherwise} \end{cases} \quad (3.16b)$$

$$(u_{mz})_{Q^*}^n = \begin{cases} 0, & \text{if } \theta_{ml} = 0, \quad (l = 1, 2, 3, 4, 5, 6, 7, 8) \\ \sum_{k=1}^8 [(W_m^{(k)})^\alpha u_{mz}^{(k)}] / \sum_{k=1}^8 (W_m^{(k)})^\alpha, & \text{otherwise} \end{cases} \quad (3.16c)$$

where

$$W_m^{(k)} = \prod_{l=1, l \neq k}^8 \theta_{ml} \quad \theta_{ml} = \sqrt{(u_{mx}^{(l)})^2 + (u_{my}^{(l)})^2 + (u_{mz}^{(l)})^2} \quad (3.17)$$

with  $l = 1, 2, 3, 4, 5, 6, 7, 8$ , and  $m = 1, 2, 3, 4, 5$ .  $\alpha$  is an adjustable parameter and usually,  $\alpha = 1$  or  $2$ . As in section 2.3, we can get the similar remarks as in two-dimensional equations.

#### 4. Numerical Results

In order to demonstrate the capabilities of the present scheme, the following flow problems are calculated: (1) oblique shock reflection on a flat plate, (2) a shock over a wedge, and (3) three-dimensional detonation wave propagation. Details of these testing problems and the numerical results by the present CE/SE method are provided in the following sections.

##### 4.1 Shock Reflection on a Flat Plate

This testing problem was proposed by Yee et al. [15]. By imposing suitable upstream boundary conditions, an oblique shock is reflected on a flat plate. The computational domain is  $[4.0 \times 1.0]$ . The flow conditions are:

Ahead of shock:

$$(u, v, \rho, p) = (2.9, 0.0, 1.0, 0.71428)$$

Behind the shock:

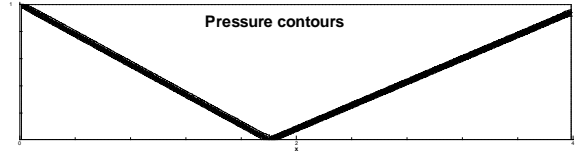
$$(u, v, \rho, p) = (2.6193, -0.50632, 1.7, 1.5282) \quad (4.1)$$

where  $u$  and  $v$  are the  $x$  and  $y$  components of velocity,  $\rho$  is density, and  $p$  is pressure. The flow condition before the incident shock is imposed on the left lateral boundary. The after-shock condition is imposed on the top horizontal boundary. The lower horizontal boundary is a solid wall, where a reflective condition is used. The right lateral boundary is a supersonic outlet, and a non-reflective condition is imposed. Note that the details of the non-reflective condition treatment in setting of the CE/SE method can be found in reference [8]. The analytical solution of the reflected shock is provided in [15].

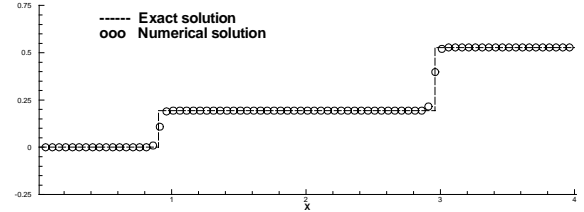
The computational domain is decomposed into 19200 uniform quadrilaterals. Because a structured mesh is used in this calculation, only half of these mesh

points, i.e. 9600 quadrilaterals, are used for time marching in each half time step. Figure 4.1(a) shows the pressure contours, calculated by the present scheme. The angle of the reflected shock is  $23.28^\circ$ , which compares well with the analytical solution. Figure 4.1(b) shows the distribution of the pressure coefficient,  $C_p$ , at the mid-section of the computation domain. The pressure coefficient is defined as

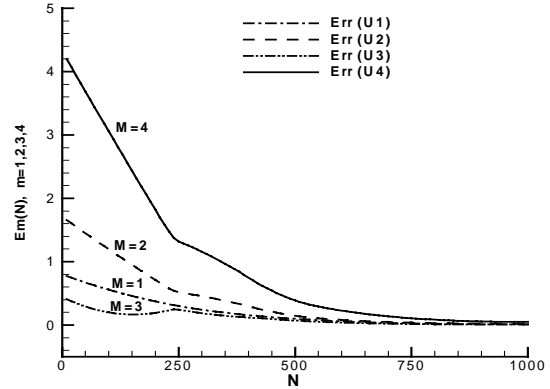
$$C_p = \frac{2}{\gamma M_\infty^2} \left( \frac{p}{p_\infty} - 1 \right) \quad (4.2)$$



(a)



(b)



(c)

Fig. 4.1: The Euler solution of a steady-state shock reflection problem: (a) pressure contours; (b) pressure coefficient distribution at the mid-section of the computation domain ( $y=0.5$ ); and (c) Convergence histories for  $U_m$ ,  $m=1, 2, 3, 4$ .

The numerical result here shows that the pressure jump condition agrees well with the analytical solution. Note that there is only one data point in the jump condition for both incident shock and the reflected shock. In addition, the numerical resolution of the reflected shock is identical to that of the incident shock.

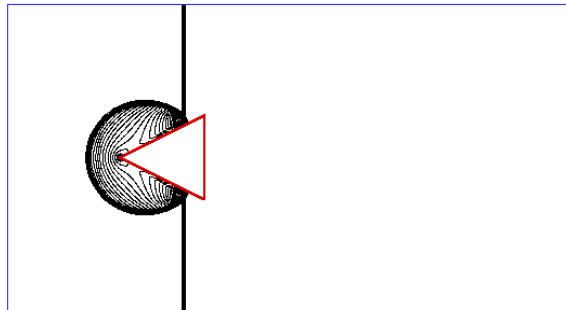
Figure 4.1(c) shows the convergence history of the four computational variables, denoted as  $u_m$ , for  $m = 1, 2, 3, 4$ . The abscissa  $N$  is the number of time steps, and the ordinate is the errors, which are defined as the difference between numerical results and analytical solutions, i.e.,

$$E_m(n) = \left\{ \sum_{j=1}^{N_c} [(u_m)_j^n - \hat{u}_m] \right\} / N_c \quad (4.3)$$

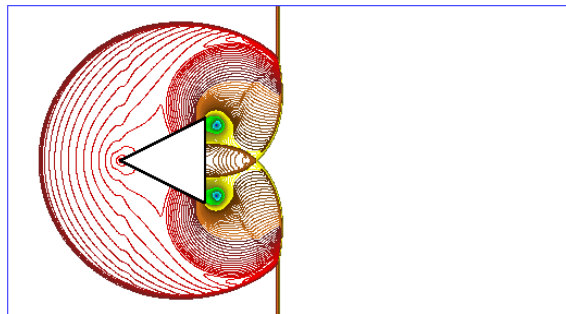
where  $\hat{u}_m$  is the analytical solution, and  $N_c$  is the number of mesh points employed in the present calculation. Figure 4.1(c) shows that numerical solutions converge to the analytical solutions monotonically except  $U_3$  near  $N = 250$  where the  $E_3$  wiggles. This is due to the incidence of the imposed oblique shock reaching the lower solid wall boundary.

#### 4.2 Shock Wave Diffraction over a Wedge

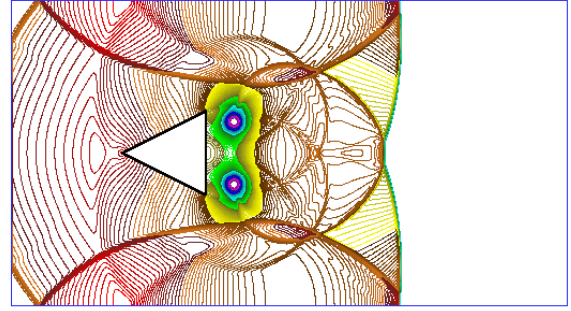
This is a flow field taken from the flow album edited by van Dyke [16]. A planar shock wave at  $M_a=1.3$  moves towards a wedge of  $\theta = 26.565^\circ$ . Only half of the flow field is calculated because of the symmetric condition. The computational domain is  $[-0.8, 3.2] \times [0, 1.1]$ , excluding the wedge. The whole domain is decomposed into 66,864 non-uniform quadrilaterals. Here a structured mesh is used, so only half of mesh points are used for time marching in each half-time step. To enhance the visual effect, the solution of the full domain is presented in Fig. 4.2.



(a)  $t=0.725$



(b)  $t=1.2125$



(c)  $t=1.825$

Fig. 4.2: Density contours at three different times compared with the experimental photographs.

At  $t = 0$ , the incident planar shock wave is placed at  $x = -0.5$ . A slip and reflective condition is imposed on upper and lower horizontal boundaries. Note that the lower horizontal boundary is the symmetric central line. The slip and reflective condition is also imposed on the surfaces of the wedge. The right lateral boundary is a supersonic outlet, where the non-reflective condition is imposed.

Figure 4.2 shows the density contours at three different times. When the planar shock reaches the wedge, a circular reflection wave is generated. As the shock passes the wedge, flow field separates and forms vortices around the two sharp corners. Further interaction between shock and vortices produces increasingly elaborate patterns of shock waves, slip lines and vortices. These results agree well with the experiment result [16] in flow pattern except those phenomena induced by the viscous effect. Here, it should be point out that the size of the experimental photos is a little smaller than that of the numerical figures.

#### 4.3 Three-Dimensional Detonation

The present scheme has been extended for solutions of conservation laws with source terms. Previously, we have reported numerical simulations of one- and two-dimensional detonation waves by using the CE/SE method [17]. Those results have been validated by compared with analytical solutions and previously numerical solutions reported by other numerical analysts. In the present paper, a three-dimensional simulation of detonation wave is performed by solving the reacting Euler equations. The chemical reactions are modeled by single-step, irreversible, finite-rate kinetics. Two chemical species are consider, i.e., the reactant and product. One species equation is added to the Euler equations and solved simultaneously. After proper non-dimensionalization, the controlling parameters of this detonation wave are the overdriven factor  $f$ , the specific heat ratio  $\gamma$ , the activation energy  $E^+$ , and the

heat release rate  $q_0$ . In the present calculation,  $f = 1.6$ ,  $\gamma = 1.2$ ,  $E^+ = 50$ , and  $q_0 = 50$ .

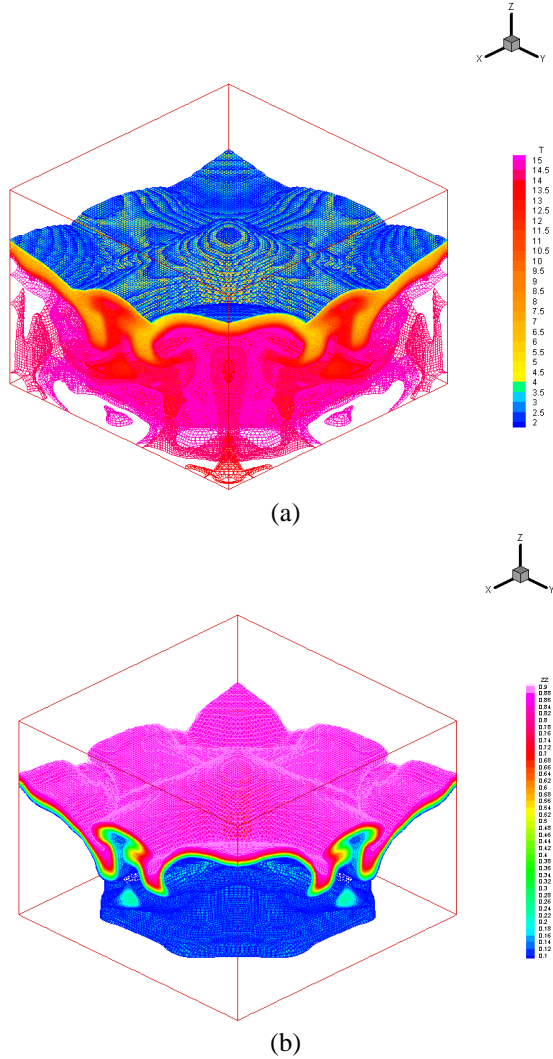


Fig. 4.3: A simulated three-dimensional detonation wave in a square duct: (a) temperature contours, and (b) product species contours.

The computation domain is  $[8 \times 8 \times 6]$ , which is decomposed into 6.4 millions hexahedrons. Since a structured mesh is used, only half of the mesh points (i.e., 3.2 millions hexahedrons) are used for time marching in each half-time step. Reflective wall condition is imposed on the four lateral boundaries. The fresh reactant travels from top to bottom, and is consumed by the flame front. On the top surface, the incoming flow condition is specified. On the bottom surface, a non-reflective boundary condition is imposed. The coordinate system is chosen such that the flame front stays around  $z=0.5$  section of the computational domain.

Figure 4.3 shows snap shots of temperature and product species contours. The flow field is composed of the quiescent state of the reactant before the shock, a flame zone with finite rate reaction, and the equilibrium state after the reaction zone. Due to cellular structure of the detonation, the flow field is very complex. The shock front is characterized by mushroom-shaped incident shocks interacting with a Mach stem. The width of the Mach stem changes in a periodic fashion and many strong vortices are created during the process. We observe the classical picture of “explosion within explosions,” sustained by the propagation of the transverse cells in the detonation front. The contours show high temperature regions around triple points. At each collision of triple points, vortices with opposite signs will be created and propagated downstream. Due to these vortices, unburned reactant is engulfed into the flame zone and the unburned pockets behind the flame zone are created. The continuous burning of the unburned pockets behind the flame zone greatly extended the effective flame zone.

### Concluding Remarks

In this paper, a modified space-time CE/SE method for two- and three-dimensional Euler equations are introduced. In the present method, only one conservation element (CE) is employed at each grid point. Space-time flux conservation is enforced over the CE to calculate the flow variables  $u_m$ . As a contrast to Chang’ original CE/SE method, the calculation of the spatial gradients of the flow variables is not based on the principle of space-time flux conservation. Instead, a central difference reconstruction procedure is employed to calculate them. As a result, quadrilaterals and hexahedron are used as the basic mesh elements for the two- and three-dimensional Euler equations, respectively. This arrangement can be illustrated as a straightforward extension of the CE/SE method for the one-dimensional equations. It should be noted that the two- and three-dimensional formulations of the present scheme are general and suitable for structured as well as unstructured meshes.

Nevertheless, the present modified space-time CE/SE schemes retain most of the favorable features of the original CE/SE method, including the unified treatment of space and time, accurate computation of space-time flux conservation, and high-fidelity resolution of unsteady flow field. The capabilities of the present method are demonstrated by the numerical results of several standard flow problems. It is shown that the present scheme is accurate in capturing shocks and vortices, and very robust.

## References

1. S.C. Chang and W.M. To, A New Numerical Framework for Solving Conservation Laws – The Method of Space-Time Conservation Element and Solution Element, NASA TM 104495, August 1991.
2. S.C. Chang, The Method of Space-Time Conservation Element and Solution Element – A New Approach for Solving the Navier Stokes and Euler Equations, *J. Comput. Phys.*, **119**, 295 (1995).
3. S.C. Chang, S.T. Yu, A. Himansu, X.Y. Wang, C.Y. Chow and C.Y. Loh, The Method of Space-Time Conservation Element and Solution Element – A New Paradigm for Numerical Solution of Conservation Laws, *Computational Fluid Dynamics Review*, **1**, 206 (1998), Edited by M. Hafez and K. Oshima, World Scientific Publisher.
4. S.C. Chang, X.Y. Wang and C.Y. Chow, The Space-Time Conservation Element and Solution Element Method: A New High-Resolution and Genuinely Multidimensional Paradigm for Solving Conservation Laws, *J. Comput. Phys.*, **156**, 89 (1999), jcph.1999.6354.
5. S.C. Chang, X.Y. Wang and W.M. To, “Application of the Space-Time Conservation Element and Solution Element Method to One-Dimensional Convection-diffusion Problems,” *J. Comput. Phys.*, **165**, 189 (2000), jcph.2000.6610.
6. X.Y. Wang and S.C. Chang, A 2D Non-Splitting Unstructured Triangular Mesh Euler Solver Based on the Space-Time Conservation Element and Solution Element Method, *Computational Fluid Dynamics Journal*, **8**, 309 (1999).
7. X.Y. Wang and S.C. Chang, A 3-D Non-Splitting Structured/Unstructured Euler Solver Based on the Space-Time Conservation Element and Solution Element Method, AIAA Paper 99-3278.
8. S.C. Chang, A. Himansu, C.Y. Loh, X.Y. Wang, S.T. Yu, P. Jorgenson, Robust and Simple Nonreflecting Boundary Conditions for the Space-Time Conservation Element and Solution Element Method, AIAA Paper 97-2077.
9. Z.C. Zhang and M.Y. Shen, New Approach to Obtain Space-Time conservation Schemes,” *Chinese J. of Aeronautics*, **10**, 87 (1997).
10. Z.C. Zhang and M.Y. Shen, Improved Scheme of Space-Time Conservation Element and Solution Element, *J. of Tsinghua University (Sci & Tech )*, **37**, 65(1997).
11. Z.C. Zhang, A New General Space-Time Conservation Scheme for 2D Euler Equations,” *Chinese J. of Computational Mechanics*, **14**, 377 (1997).
12. Z.C. Zhang and M.Y. Shen, New Space-Time Conservation Schemes for Solving 2-D Euler Equations, *ACTA MECHANICA SINICA*, **31**, 152 (1999).
13. Z.C. Zhang and S.T. Yu, Shock Capturing without Riemann Solver---A Modified Space-Time CE/SE Method for Conservation Laws, AIAA Paper 99-0904.
14. C. Zhang, S.T. Yu, S.C. Chang, A. Himansu and P. Jorgenson, A Modified Space-Time CE/SE Method for Euler and Navier-Stokes Equations, AIAA Paper 99-3277.
15. H.C. Yee, R.F. Warming and A. Harten, Implicit Total Variation Diminishing (TVD) Schemes for Steady-State Calculations, AIAA paper 83-1902.
16. M. Van Dyke, An Album of Fluid Motion, The Parabolic Press, Stanford, California, 1988.
17. S.J. Park, S.T. Yu and M.C. Lai, Numerical Calculation of Unstable Detonations by the Method of Space-Time Conservation Element and Solution Element, AIAA paper 99-0491.